Structure and Assembly of the Nup84p Complex

Symeon Siniossoglou,* Malik Lutzmann,* Helena Santos-Rosa,* Kevin Leonard,‡ Shirley Mueller,§ Ueli Aebi,§ and Ed Hurt*

*Biochemie-Zentrum Heidelberg, D-69120 Heidelberg, Germany; ‡European Molecular Biology Laboratory, D-69117 Heidelberg, Germany; and §Biozentrum, Maurice E. Müller Institute for Structural Biology, CH-4056 Basel, Switzerland

Abstract. The Nup84p complex consists of five nucleoporins (Nup84p, Nup85p, Nup120p, Nup145p-C, and Seh1p) and Sec13p, a bona fide subunit of the COPII coat complex. We show that a pool of green fluorescent protein–tagged Sec13p localizes to the nuclear pores in vivo, and identify *sec13* mutant alleles that are synthetically lethal with *nup85Δ* and affect the localization of a green fluorescent protein–Nup49p reporter protein. In the electron microscope, *sec13* mutants exhibit structural defects in nuclear pore complex (NPC) and nuclear envelope organization. For the assembly of the complex, Nup85p, Nup120p, and Nup145p-C are essential. A highly purified Nup84p complex was isolated from yeast under native conditions and its molecular mass was determined to be 375 kD by quantitative scanning transmission electron microscopy and analytical ultracentrifugation, consistent with a monomeric complex. Furthermore, the Nup84p complex exhibits a Y-shaped, triskelion-like morphology 25 nm in diameter in the transmission electron microscope. Thus, the Nup84p complex constitutes a paradigm of an NPC structural module with distinct composition, structure, and a role in nuclear mRNA export and NPC biogenesis.

Key words: nuclear pore complex • nuclear envelope • Nup84p • Sec13p • electron microscopy

Introduction

In eukaryotic cells, transport between the nucleus and cytoplasm takes place through the nuclear pore complexes (NPCs)[1] (Ohno et al., 1998). EM combined with image reconstruction has revealed many structural details of the NPC framework (for review see Stoffler et al., 1999). Accordingly, one of the most prominent NPC substructures is the central spoked ring, which exhibits eightfold symmetry and is embedded within the plane of the double nuclear membrane. The spoke complex is embraced by two ring assemblies that face the nuclear and cytoplasmic sites of the nuclear envelope, respectively. The cytoplasmic ring carries eight globular particles, from which eight short fibrils protrude into the cytoplasm. The nuclear ring is capped by a highly regular structure called the nuclear basket. Although the known vertebrate nucleoporins do not exhibit high sequence homology with their yeast counterparts, the overall NPC structure (spoke complex and outer and inner rings) is conserved between yeast and vertebrates (Yang et al., 1998). Furthermore, peripheral structural elements such as cytoplasmic fibrils, nuclear baskets, and NPC-attached intranuclear filaments were recently reported to be also present in yeast NPCs as revealed by EM (Fahrenkrog et al., 1998; Strambio-de-Castillia et al., 1999).

The molecular dissection of the yeast NPC is close to completion, i.e., most of the yeast nucleoporins are known to date. This fast progress was possible because multiple sources of information, e.g., yeast genetic screens with nucleoporin mutants, affinity-purification of tagged nucleoporins, and identification of their associated partner proteins, a NPC isolation procedure, and completion of the yeast genome sequencing project, could be successfully combined (for reviews see Rout and Wente, 1994; Doye and Hurt, 1997; Fabre and Hurt, 1997). When nucleoporin mutants are analyzed for an altered NPC structure and function, two distinct phenotypical defects become apparent: (a) inhibition of nucleocytoplasmic transport reactions such as nuclear mRNA export or nuclear protein import; and (b) structural abnormalities of the NPCs and the nuclear membrane. Interestingly, distinct nucleoporin mu-

Address correspondence to Ed Hurt, Biochemie-Zentrum Heidelberg, University of Heidelberg, Im Neuenheimer Feld 328, D-69120 Heidelberg, Germany. Tel.: 49-6221-54-4173. Fax: 49-6221-54-4369. E-mail: cg5@ix.urz.uni-heidelberg.de

The present address of S. Siniossoglou and H. Santos-Rosa is Medical Research Council Laboratory of Molecular Biology, Division of Cell Biology, Hills Road, Cambridge CB2 2QH, UK.

[1]*Abbreviations used in this paper:* GFP, green fluorescent protein; NPC, nuclear pore complex; ProtA, protein A; STEM, scanning transmission EM; TEV, tobacco etch virus; ts, temperature-sensitive.

tants exhibit both defects, whereas others have only transport or structural defects, respectively. To the first category belong several members of the Nup84p complex, a large assembly that consists of Nup84p, Nup85p, Nup120p, Nup145p-C, Seh1p, and Sec13p. Nucleoporin members of this complex exhibit nuclear mRNA export defects, but not inhibition of nuclear protein import (Aitchison et al., 1995; Goldstein et al., 1996; Siniossoglou et al., 1996; Teixeira et al., 1997). Therefore, it was suggested that the Nup84p complex is linked to the mRNA export machinery, consistent with the recent finding that Nup85p interacts with the mRNA exporter complex Mex67p–Mtr2p (Segref et al., 1997; Santos-Rosa et al., 1998). However, the Nup84p complex is also linked to the biogenesis pathway of NPCs, since mutation of members of the Nup84p complex causes severe defects in the organization and distribution of NPCs within the nuclear envelope. The most apparent phenotype is NPC clustering, connected with nuclear envelope abnormalities such as long nuclear membrane extensions, which penetrate deeply into the cytoplasm (Siniossoglou et al., 1996). A different structural defect associated with *nup116* and *gle2* mutants is a nuclear membrane seal over the NPCs (Wente and Blobel, 1993; Murphy et al., 1996; Bailer et al., 1998). Thus, nucleoporins have specific roles in the biogenesis, distribution, and structural integrity of NPCs and nucleocytoplasmic transport.

In contrast to transport routes through the pores, little is known about how NPCs assemble and become incorporated into the nuclear membrane. Progress has been made in the *Xenopus* oocyte system, which can be used to study and manipulate NPC assembly (Goldberg et al., 1997), but mechanistic aspects still remain unknown. Interesting in this context is the finding that the Nup84p complex contains one unexpected protein, Sec13p, which could point to a vesicular biogenesis step during NPC formation. Sec13p is a subunit of the COPII complex, which is involved in vesicle transport from the ER to the Golgi apparatus (Kaiser and Ferro-Novick, 1998).

Here, we have further investigated the role of the bona fide COPII coat subunit, Sec13p, as the most unexpected member of the Nup84p complex. We show that a pool of Sec13p colocalizes with clustered NPCs in *nup133*$^-$ cells. Furthermore, *sec13* temperature-sensitive (ts) alleles were obtained that are genetically linked to *NUP85* and exhibit an abnormal NPC organization. Gel filtration chromatography revealed that Sec13p is a specific member of the large Nup84p complex. Finally, we demonstrate by negative staining and rotary shadowing that the highly purified Nup84p complex exhibits a distinct Y-shaped structure with an average diameter of 25 nm.

Materials and Methods

Yeast Strains, Microbiological Techniques, Plasmids, and DNA Manipulations

The yeast strains used in this study are listed in Table I. For construction of double disruption strains, haploid strains of opposite mating type and carrying the indicated gene disruptions and gene mutations with an appropriate shuffle plasmid (*URA3* containing *ARS/CEN* plasmid) were mated. The haploid strain RSY282 (kindly provided by Dr. Randy Schekman, University of California, Berkeley, Berkeley, CA), which harbors the *sec23-1* mutation, was mated to strain RS453 of opposite mating type. Diploids growing on selective medium were sporulated, and after tetrad analysis haploid double mutants were selected. Standard DNA manipulations (restriction analysis, end filling, ligation, PCR amplification, and DNA sequencing) and microbiological techniques (growth and transformation of yeast and *E. coli* strains, plasmid recovery, mating, and tetrad analysis) were done as described earlier (Siniossoglou et al., 1996). The following plasmids were used: pUN100, *ARS1/CEN4* plasmid with the *LEU2* marker; pRS314 and pRS316, *ARS4/CEN6* plasmids with the *TRP1* and *URA3* markers, respectively; pASZ11-ADE2-green fluorescent pro-

Table I. Yeast Strains

	Yeast strains
RS453	*MATa/α,ade2/ade2,his3/his3,leu2/leu2,trp1/trp1,ura3/ura3*
NUP120-ProtA	*Mata,ade2,his3,leu2,trp1,ura3,nup120::HIS3* (pRS315-LEU2-NUP120-ProtA)
NUP84-ProtA	*Mata,ade2,his3,leu2,trp1,ura3,Δnup84::HIS3* (pUN100-LEU2-NUP84-ProtA)
nup84$^-$	*MATa,ade2,his3,leu2,trp1,ura3,nup84::HIS3*
nup85Δ	*MATa,ade2,his3,leu2,trp1,ura3,Δnup85::HIS3* (partial disruption/deletion)
seh1$^-$	*MATa,ade2,his3,leu2,trp1,ura3,seh1::HIS3*
SEC13 shuffle	*MATa,ade2,his3,leu2,trp1,ura3,sec13::HIS3* (pRS316-URA3-SEC13-Myc)
ProtA-NUP85	*MATa,ade2,his3,leu2,trp1,ura3,Δnup85::HIS3* (pUN100-LEU2-ProtA-NUP85)
NUP84-ProtA	*MATa,ade2,his3,leu2,trp1,ura3,nup84::HIS3* (pUN100-LEU2-NUP84-ProtA)
ProtA-TEV-NUP85	*MATa,ade2,his3,leu2,trp1,ura3,nup85::HIS3* (pUN100-LEU2-ProtA-TEV-NUP85)
seh1(Δ248-288)-ProtA	*MATa,ade2,his3,leu2,trp1,ura3,seh1::HIS3* (pRS315-LEU2-seh1 (Δ248-288)-ProtA)
SEC13-GFP	*MATa,ade2,his3,leu2,trp1,ura3,sec13::HIS3* (pUN100-LEU2-SEC13-GFP)
SEC13-GFP/nup133$^-$	*MATa,ade2,his3,leu2,trp1,ura3,sec13::HIS3,nup133::HIS3* (pUN100-LEU2-SEC13-GFP)
sec13-3	*MATa,ade2,his3,leu2,trp1,ura3,sec13::HIS3* (pUN100-LEU2-sec13-3)
SEC13-ProtA	*Mata,ade2,his3,leu2,trp1,ura3,sec13::HIS3* (pUN100-LEU2-SEC13-ProtA)
SEC13/seh1$^-$	*MATa,ade2,his3,leu2,trp1,ura3,sec13::HIS3,seh1::HIS3* (pRS316-URA3-SEC13-Myc)
SEC13/nup84$^-$	*MATa,ade2,his3,leu2,trp1,ura3,sec13::HIS3,nup84::HIS3* (pRS316-SEC13-Myc)
SEC13/nup85Δ	*MATa,ade2,his3,leu2,trp1,ura3,sec13::HIS3,nup85Δ::HIS3* (pRS316-SEC13-Myc)
sec13-34/nup85Δ	*MATa,ade2,his3,leu2,trp1,ura3,sec13::HIS3,nup85Δ::HIS3* (pUN100-LEU2-sec13-34)
sec13-14/nup85Δ	*MATa,ade2,his3,leu2,trp1,ura3,sec13::HIS3,nup85Δ::HIS3* (pUN100-LEU2-sec13-34)
SEH1-ProtA	*MATa,ade2,his3,leu2,trp1,ura3,seh1::HIS3* (pRS316-URA3-SEH1-ProtA)
sec13-3/NIC96-GFP	*MATa,ade2,his3,leu2,trp1,ura3,sec13::HIS3,nic96::HIS3* (pUN100-LEU2-sec13-3,pRS314-TRP1-NIC96-GFP)
sec23-1	*MATα,ade2,his3,leu2,trp1,ura3,sec23-1*
NUP145-ProtA	*MATa,ade2,his3,leu2,trp1,ura3,nup145::HIS3* (pUN100-LEU2-NUP145-C-ProtA)

tein (GFP)-NUP49, a SacI/BamHI fragment containing the *NUP49–GFP* fusion was inserted into the SacI/BamHI site of pASZ11-ADE2; and pASZ11-ADE2-GFP-PUS1 (Siniossoglou et al., 1998).

Construction of Fusion Genes and NUP85 and SEH1 Truncation Mutants

To construct protein A (ProtA)-TEV-Nup85p, which contains the tobacco etch virus (TEV) protease cleavage site (ENLYFQG) between the *ProtA* tag and *NUP85* ORF, an NdeI site was generated with a primer that hybridizes at the ATG start codon of *NUP85* (5′-TTT TTC ATA TGA CAA TCG ATG AT-3′), and with the help of an internal primer hybridizing 1.32 kb after the initiator ATG, a PCR fragment was generated and digested with NdeI/SalI. The resulting fragment was subcloned into the NdeI/SalI sites of the pROEX-1 vector (GIBCO BRL Life Technologies). The NdeI site in this vector is six nucleotides downstream of the last codon coding for the TEV recognition site. An EcoRV site, nine nucleotides upstream of the first codon coding for the TEV site, was used to release an EcoRV/SalI fragment from the pROEX-1-TEV-*NUP85* (NdeI/SalI) construct. This fragment, containing the TEV site and part of the *NUP85* ORF, was inserted into a pBluescript vector containing the *NOP1* promoter joined to the ProtA tag, cut with EcoRV/SalI. This pBS-NOP1::ProtA-TEV-NUP85 (NdeI/SalI) construct was finally cut with SacI/NcoI to release a *NOP1::ProtA-TEV-NUP85* (SacI/NcoI) fragment and was then ligated into a pUN100-NUP85 plasmid, previously cut with SacI/NcoI. The *TEV-NUP85* junction in the final pUN100-ProtA-TEV-NUP85 was verified by DNA sequencing. For the construction of the SEC13-GFP and SEH1-GFP fusions, the pUN100-SEC13-ProtA and pRS316-SEH1-ProtA plasmids (Siniossoglou et al., 1996) were digested with BamHI and the sequence coding for the ProtA tag was replaced by a BamHI GFP cassette encoding the S65T/V163A variant of the GFP.

For the construction of the ProtA-Nup85pΔN truncation mutant, a 1.7-kb DraI fragment encoding residues 82–744 plus 70 bp from the 3′ untranslated region was subcloned into pBluescript-pNOP1-ProtA, cut with HindIII, and blunt-ended. The resulting plasmid coded for an NH_2-terminal tagged ProtA-Nup85p-C in which the L in position 82 (TTA) was kept (CTA) (LNCLR-QAFM). The sequence of the junction between the ProtA and the COOH-terminal portion of Nup85p is LQEFDIKL. Next, a 2.8-kb BamHI/XhoI fragment containing the *NOP1::ProtA-NUP85-C* fragment was subcloned into pRS314-TRP1, cut with BamHI/HindIII. To construct a ProtA-Nup85ΔCp mutant, a 2.25-kb SacI/partial-BglII fragment containing the pNOP1-ProtA cassette plus the first 453 amino acid residues of Nup85p (MTI-NEMLED) was subcloned from pUN100-NOP1::ProtA-NUP85 (Siniossoglou et al., 1996) into a pRS315-LEU2 vector and cut with SacI/BamHI. Next, a SmaI terminator sequence, containing several stop codons in the three possible reading frames, was cloned into the BglII-adjacent SmaI site of the poly-linker.

Isolation of sec13 ts Alleles

The *SEC13-ProtA* fusion gene was amplified by PCR under conditions that impair the fidelity of the *Taq* DNA polymerase. The buffer conditions were 6.5 mM $MgCl_2$, 0.5 mM $MnCl_2$, 1 mM dGTP, dCTP, dTTP, and 0.2 mM dATP. Around 20 ng of template DNA and 5 U of *Taq* polymerase were used. The PCR product was gel-purified and digested with SacI/HindIII to release the *SEC13-ProtA* fragment and to insert it in a pUN100-LEU2, cut with SacI/HindIII. The ts library was first transformed into *E. coli* and 5,000 transformants were obtained from which the plasmid DNA was isolated. 78% of the plasmids had *SEC13-ProtA* inserts, with a mutagenesis rate of 2% as judged by DNA sequencing of six randomly selected clones. The *sec13::HIS3* disrupted strain complemented by pRS316-SEC13-Myc was transformed with the pUN100-LEU2-SEC13-ProtA library. About 2,200 yeast transformants selected on SDC-ura-leu plates were replica-plated on 5-fluoro-orotic acid plates. The 800 colonies that were growing on 5-fluoro-orotic acid were plated on yeast extract–peptone–D-glucose and tested for thermosensitive growth at 37°C. Finally, 17 *sec13* mutants with a thermosensitive growth defect at 37°C were obtained.

Affinity-Purification of ProtA Fusion Proteins, TEV Cleavage, and Gel Filtration

Affinity-purification of ProtA fusion proteins by IgG-Sepharose chromatography was done according to Siniossoglou et al. (1998). 15 g of spheroplasts derived from the *nup85::HIS3* strain and complemented by plasmid-borne *ProtA-TEV-NUP85* was used for the purification. To isolate the Nup84p complex under native conditions, the ProtA-TEV-Nup85p fusion protein was isolated by IgG-Sepharose chromatography as described (Siniossoglou et al., 1998). However, instead of eluting at acidic pH, a second washing of the IgG-Sepharose beads was performed using 5 ml TEV cleavage buffer (0.01% Triton X-100, 50 mM Tris-HCl, pH 8.0, 150 mM NaCl, 1 mM EDTA). The Sepharose beads were then incubated in 200–500 μl of cleavage buffer containing 0.7 mM DTT and 10 U of recombinant TEV protease (Life Technologies) per gram of lysed cells for 70 min on a rotating wheel at 16°C. The supernatant containing the TEV protease–released nucleoporin complex was collected by centrifugation, and the beads were washed once with cleavage buffer before a final elution with 1 ml of 0.5 M acetic acid, pH 3.4. For gel filtration chromatography, the TEV-derived supernatant was concentrated by ultrafiltration (Nano-Spin Plus; Gelman) and applied onto a Superdex 200 gel filtration column connected to an FPLC system (Amersham Pharmacia Biotech). Samples were chromatographed in 150 mM NaCl, 50 mM Tris-HCl, pH 8.0, 1 mM EDTA. The flow rate was 0.3 ml/min and 0.6-ml fractions were collected. 25 μl of each fraction was analyzed by SDS-PAGE followed by silver-staining or Western blotting using antibodies specific for the different components of the Nup84p complex.

EM

Glycerol spraying/low-angle rotary metal shadowing of the highly purified Nup84p complex was performed as described (Häner et al., 1997). For negative staining, a 10-μl drop of sample was placed on a carbon-collodion–coated grid that had been freshly glow-discharged in air. After washing with 100 μl of buffer, the sample was stained by washing with 100 μl of 1% (wt/vol) aqueous uranyl acetate and blotted dry. Micrographs were taken at 80 kV in a Philips 400T electron microscope at a magnification of 36,000. Thin section EM of yeast *sec13* ts mutants was done as described in Segref et al. (1997).

Molecular Mass Determination of the Isolated Nup84p Complex

For mass measurement by scanning transmission EM (STEM), 5-μl aliquots of the sample were adsorbed for 1 min to glow discharged thin carbon films that spanned a thick fenestrated carbon layer covering 200-mesh/inch gold-plated copper grids. The grids were then blotted and washed (with subsequent blotting) on five drops of 100 mM ammonium acetate, which had been prepared using quartz bidistilled water. They were then immediately frozen in liquid nitrogen and freeze-dried at −80°C overnight in the STEM. A Vacuum Generators STEM HB-5 interfaced to a modular computer system (D-8035 Gauting; Tietz Video and Image Processing Systems GmbH) was employed. Details of the instrument's calibration for mass measurement may be found in Engel (1978) and Müller et al. (1992). Annular dark-field images were recorded digitally from the unstained freeze-dried samples at 80 kV accelerating voltage. The nominal magnification was 200,000 and recording doses were in the range of 300 electrons/nm^2. The 512 × 512 pixel images were evaluated using the program package IMPSYS as outlined in Engel and Reichelt (1988) and Müller et al. (1992). The mass values were corrected for beam-induced mass loss (Müller et al., 1992) according to the behavior of other proteins in their mass range (our unpublished data). The resulting absolute values were then displayed in histograms and fitted by Gauss curves.

Sedimentation velocity and low-speed sedimentation equilibrium runs of the purified Nup84p complex were performed on an Optima XLA analytical ultracentrifuge (Beckman Instruments) equipped with an absorption optical system (Terzi et al., 1994). The sample was analyzed at 8°C (sedimentation velocity) or 4°C (sedimentation equilibrium) in 50 mM Tris-HCl, pH 8.0, containing 300 mM NaCl, 0.5 mM DTT, and 1.5 mM DTT, with the protein concentration adjusted to OD_{280} ranging between 1.0–0.1. Sedimentation velocity runs were performed at 52,000 rpm in a 12-mm epon double-sector cell, which was filled with 0.12 ml sample in one sector and the same volume of buffer in the other. Sedimentation coefficients were corrected to water by a standard procedure (Eason, 1986). Sedimentation equilibrium runs were performed at 6,400, 7,200, and 8,000 rpm and at protein concentrations adjusted to OD_{280} of 1.0, 0.2, and 0.15. An average molecular mass was determined using linear regression analysis so as to obtain the best linear fit of logarithmus A versus r^2 plots. A partial specific volume of 0.73 ml/g was used for the calculations.

Miscellaneous

SDS-PAGE and Western blot analysis were performed according to Siniossoglou et al. (1996). In situ hybridization of poly(A)$^+$ RNA, indirect immunofluorescence using anti-Nsp1p antibodies, and fluorescence microscopy of GFP-labeled yeast cells were performed according to Santos-Rosa et al. (1998).

Results

A Pool of GFP-tagged Sec13p Localizes In Vivo to the Nuclear Pores

Sec13p is a component of the COPII coat complex in yeast and is involved in vesicular transport (Salama et al., 1993; Barlowe et al., 1994; Kaiser and Ferro-Novick, 1998). In addition, Sec13p was found to coenrich with the Nup84p nucleoporin complex (Siniossoglou et al., 1996). To find out whether Sec13p can be detected at the nuclear pores in living cells, a GFP-tagged *SEC13* under the control of its authentic promoter was expressed as a functional fusion protein in the otherwise lethal *sec13::HIS3* null mutant. Sec13p-GFP exhibits both a punctate nuclear/ER membrane and cytoplasmic staining (Fig. 1 a). The Sec13-GFP signal in the cytoplasm tends to be concentrated in spots underlying the plasma membrane, which is suggestive of the peripheral ER. In contrast, GFP-tagged Seh1p predominantly stained the nuclear envelope with little staining in the cytoplasm, thus having characteristics of a classical NPC protein (Fig. 1 a). Since the nuclear envelope staining of Sec13p-GFP was punctate, it is possible that this represents nuclear pore labeling. We therefore used the *nup133::HIS3* knockout strain in which the NPCs lose

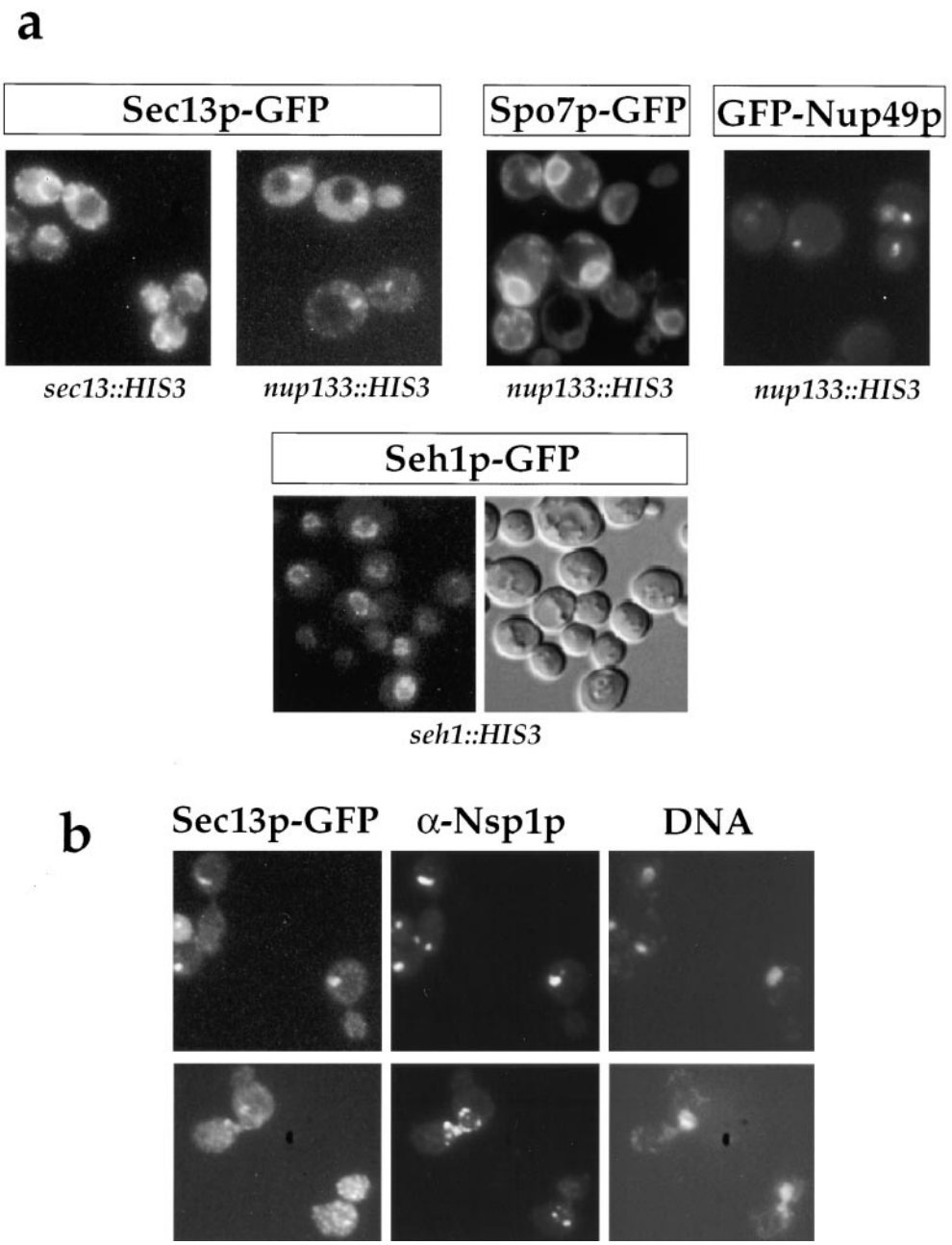

Figure 1. A pool of Sec13p-GFP localizes to the nuclear pores. (a) The *sec13*$^-$/*nup133*$^-$ double mutant complemented by either *SEC13-GFP* and *NUP133* (*sec13::HIS3*) or by *SEC13-GFP* alone (*nup133::HIS3*) was analyzed by fluorescence microscopy (upper panel). In addition, Spo7p-GFP (Siniossoglou et al., 1998) and GFP-Nup49p were tested in the *nup133*$^-$ cells (upper panel). For comparison, the *seh1::HIS3* disruption mutant complemented by plasmid-borne *SEH1-GFP* was analyzed in the fluorescence microscope (lower panel). (b) The *sec13*$^-$/*nup133*$^-$ double mutant expressing Sec13p-GFP was analyzed by indirect immunofluorescence microscopy using a monoclonal anti-Nsp1p antibody. It was also stained for DNA.

their even distribution and cluster in one or few areas within the nuclear envelope. Indeed, a pool of Sec13-GFP, like Nup49-GFP, clustered at the nuclear envelope in the *nup133*$^-$ mutant (Fig. 1 a). Indirect immunofluorescence using antibodies against the nucleoporin Nsp1p confirmed that the clustered NPCs colocalize with the Sec13p-GFP signal (Fig. 1 b). On the other hand, another nuclear membrane/ER protein, Spo7p-GFP, did not cluster with NPCs in the *nup133*$^-$ mutant (Fig. 1 b; see also Siniossoglou et al., 1998). This shows that a pool of Sec13p is specifically associated with NPCs under steady state conditions, which is in agreement with our biochemical data for the Nup84p complex (see below).

Novel Thermosensitive sec13 Mutants that Affect Distribution of the NPC Reporter GFP-Nup49p and Nuclear Morphology

Whereas the Nup members of the Nup84p complex (Nup84p, Nup85p, Nup120p, and Nup145p-C) have a function in both NPC distribution and nuclear mRNA export (Siniossoglou et al., 1996), the role of Sec13p and Seh1p within this complex remains unknown. Therefore, we screened for novel *sec13* mutants that are impaired in the organization and the distribution of NPCs within the nuclear membrane, similar to the defects seen with some of the other Nup84p complex mutants. The *SEC13* gene was mutagenized in vitro by PCR-based random mutagenesis (see Materials and Methods) and inserted into an *ARS/CEN* plasmid. Several thermosensitive *sec13* alleles were isolated from this mutagenized bank. In total, 17 ts alleles of *SEC13* (which do not allow growth at 37°C) were characterized further (for growth properties of some of these alleles, see Fig. 2 a). These *sec13* ts mutants were transformed with a plasmid encoding GFP-Nup49p, which serves as a nuclear pore reporter protein, to visualize impairment of NPC assembly (Bucci and Wente, 1998) or NPC distribution within the nuclear membrane (Belgareh and Doye, 1997). Strikingly, most of these novel *sec13* mutants show an abnormal intracellular distribution of GFP-Nup49p (as well as of Nic96p-GFP; data not shown) when shifted to the restrictive temperature. This was particularly evident for those mutants that grow slowly already at intermediate temperatures (e.g., 32°C) (Fig. 2, a and b, e.g., *sec13-3*). Other mutant alleles, which are less impaired in growth at higher temperatures (e.g., *sec13-14* and *sec13-34*), exhibit less strong defects in GFP-Nup49p distribution (Fig. 2, a and b, e.g., *sec13-34*). When GFP-Nup49p distribution was abnormal in *sec13* mutant cells, this nucleoporin reporter was often found in clusters at the nuclear membrane or aggregated in the cytoplasm. Interestingly, the nuclear morphology, as revealed by the intranuclear reporter Pus1p-GFP (Siniossoglou et al., 1998), appears normal in these *sec13* mutants (Fig. 2 b). Another COPII mutant, *sec23-1*, also displayed an irregular distribution of GFP-Nup49p (Fig. 2, a and b; *sec23-1*). However, we noticed that in the case of *sec23-1* mutant, some cells exhibit slightly elongated nuclei, although not comparable to the highly altered nuclear envelope morphology that has been recently reported for *spo7*$^-$ and *nem1*$^-$ cells (Siniossoglou et al., 1998). In conclusion, the distribution of the nuclear pore reporter GFP-Nup49p (i.e., a ring-like nuclear envelope staining) can be altered in *sec13* thermosensitive mutants.

To analyze the nuclear envelope morphology of the *sec13* mutants at the ultrastructural level, we performed thin section EM (Fig. 2 c). Structural abnormalities can be seen in these *sec13* ts mutants, which is consistent with the aberrant distribution of the GFP-Nup49p reporter (see Fig. 2 b). Remarkably, the *sec13-14* and *sec13-34* cells develop extended clusters of herniated NPCs, similar to the herniations seen in *nup116Δ* and *gle2Δ* mutants (Wente and Blobel, 1993; Bailer et al., 1998) (Fig. 2c), whereas spindle and nucleolar morphology was not altered (data not shown). However, the cells still contain normal nuclear pores in nonherniated areas of the nuclear envelope. In the *sec13-3* mutant, a particular strong ER membrane accumulation is also seen. It is therefore possible that (a) the nuclear envelope clustering of the GFP-Nup49p reporter in *sec13* ts mutants (e.g., *sec13-14* and *sec13-34*; see Fig. 2 b) corresponds to the clustered nuclear envelope herniations at the ultrastructural level, and (b) the cytoplasmic aggregates of GFP-Nup49p seen in some of the mutant *sec13* cells correspond to pore herniations at the tips of the nuclear envelope–derived ER outgrowths. Taken together the GFP-Nup49p localization and the EM data show that the nuclear envelope and NPC organization is impaired in the *sec13-3*, *sec13-14*, and *sec13-34* mutants.

The sec13-14 and sec13-34 Alleles Exhibit a Conditional Synthetic Lethal Interaction with the nup85Δ Disruption Mutation

Since some of the *sec13* ts alleles described above affect the distribution of the Nup49p nucleoporin reporter, we tested for a functional overlap with members of the Nup84p complex. A possible genetic interaction was analyzed between the novel *sec13* ts alleles and the partial *nup85Δ* disruption, which expresses a COOH-terminal portion of the protein (Siniossoglou et al., 1996), the *nup84::HIS3*, or the *seh1::HIS3* disruption (for strain constructions see Materials and Methods). It has been reported previously that the *sec13-1* ts allele, which is impaired in ER-to-Golgi transport (Pryer et al., 1993), is not synthetically lethal with the *nup85Δ* and *seh1::HIS3* alleles (Siniossoglou et al., 1996), for example. However, we noticed that two mutant alleles, *sec13-14* (data not shown) and *sec13-34* (Fig. 3 a), are synthetically lethal with *nup85Δ* at 32°C, a temperature at which the individual mutants *sec13-34*, *sec13-14*, and *nup85Δ* can grow very well (Fig. 3 a; see also Fig. 2 a). The observed synergistic growth inhibition between *sec13-34* with *nup85Δ* is specific, since the *nup84::HIS3/sec13-34* and the *seh1::HIS3/sec13-34* double mutants are viable at 32°C (data not shown). In contrast, we do not find a synthetically lethal interaction between the *seh1* null mutant and the various *sec13* mutants, although Seh1p shares significant sequence similarity with Sec13p (see also Discussion). These data show that Sec13p not only physically associates with the Nup84p complex, but that it is also functionally linked to a particular member of this subcomplex, which is Nup85p.

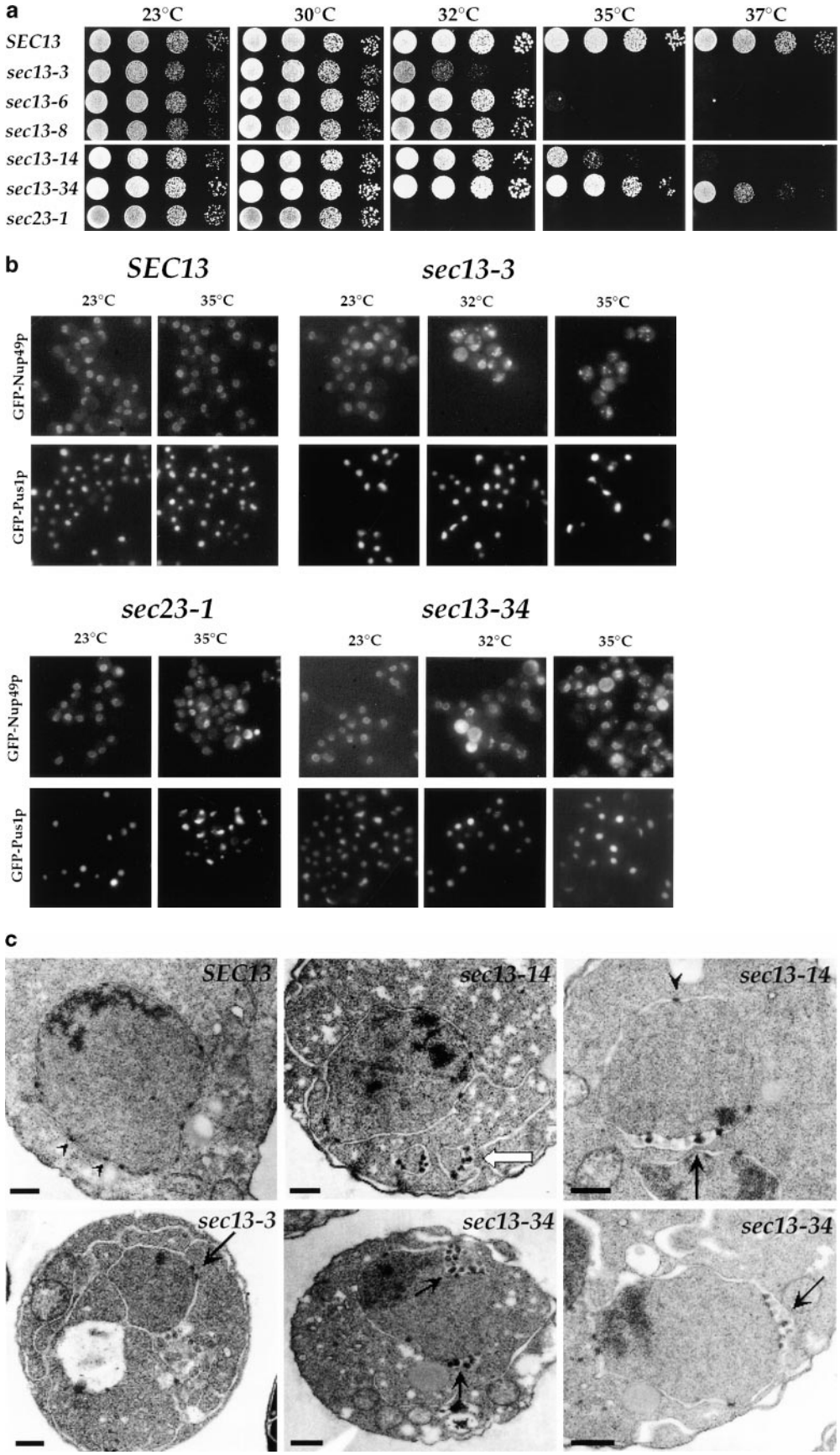

Figure 2. Novel *sec13* thermosensitive alleles that show defects in GFP-Nup49p location and nuclear membrane morphology. (a) Growth properties of novel *sec13* thermosensitive mutants. Precultures derived from the *sec13::HIS3* disrupted strain transformed with *ARS/CEN* plasmids containing the indicated *SEC13* wild-type and *sec13* ts alleles were diluted in growth medium and equivalent amounts of cells (diluted in 10^{-1} steps) were spotted onto yeast extract–peptone–d-glucose plates. All *SEC13* and *sec13* alleles are tagged with one IgG-binding domain from ProtA in their COOH termini. For control, the *sec23-1* ts mutant was also included in this analysis. It was grown for 3 d at the indicated temperatures. (b) Location of GFP-Nup49p and GFP-Pus1p in *SEC13*$^{+}$ and *sec13* and *sec23-1* ts mutants as determined by fluorescence microscopy. Cells were grown at 23°C and shifted for 5 h to either 32 or 35°C. (c) Thin-section EM of *SEC13*, *sec13-3*, *sec13-14*, and *sec13-34* cells, shifted for 5 h to 35°C. Filled arrowheads point to normal nuclear pores, arrows to nuclear envelope herniations, and the open arrow to a long nuclear membrane extension with a herniation morphology at the tip. Bars, 0.5 μm.

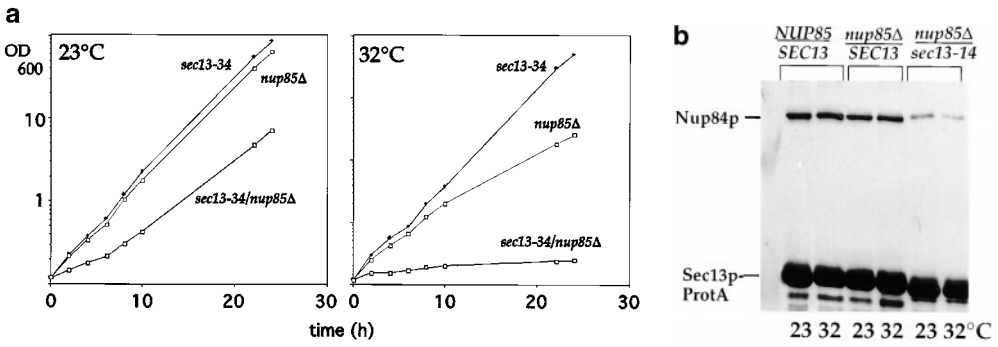

Figure 3. Genetic interaction between the *sec13-34* and *nup85*Δ mutant alleles. (a) Growth curves of the *sec13-34/nup85Δ* double mutant and of the corresponding *sec13-34* and *nup85Δ* single mutants at 23 and 32°C. The *nup85Δ* allele is derived from a partial gene disruption and expresses a Nup85p protein which is NH_2-terminally truncated (Siniossoglou et al., 1996). (b) Affinity-purification of Sec13p-ProtA from *NUP85/SEC13*, *nup85Δ/SEC13*, and *nup85Δ/sec13-14* strains grown at 23°C or shifted for 12 h to 32°C. The purified wild-type or mutant Sec13p-ProtA fusion proteins were analyzed by Western blotting using anti-Nup84p antibodies. Indicated are the positions of Sec13p-ProtA and Nup84p.

Nup145p-C, Nup120p, and Nup85p-C, but not Nup84p and Seh1p, Are Essential for Assembly of the Nup84p Complex In Vivo

To identify the essential components for Nup84p complex assembly in vivo, the Nup84p complex was purified from different mutant strains. Either Seh1p-ProtA or Nup84p-ProtA served as baits for the purification, since these two fusion proteins copurify particularly well with all components of the complex, even from cells with wild-type *SEH1* or *NUP84*. When Seh1p-ProtA was purified from the *nup84* deletion mutant, all other components of the complex, except Nup84p, were present in stoichiometric amounts (Table II). When the complex was isolated from the *seh1* deletion strain by purification of Nup84p-ProtA, all components of the Nup84p complex including Sec13p, but lacking Seh1p, were present (Table II). However, when Nup84p-ProtA was isolated from a *nup120* deletion strain, no other complex member coenriched (Table II). Seh1p-ProtA isolated from either the *nup120* disruption strain or the *nup145* deletion strain expressing only the nonessential NH_2-domain (Teixeira et al., 1997) contained substoichiometric amounts of Nup85p, but no other members of the complex. When the mutant Sec13p encoded by *sec13-14* and tagged with ProtA was affinity-purified from the partial disruption *nup85Δ* mutant (Siniossoglou et al., 1996), it largely lacked Nup84p and the other complex members (Fig. 3 b; data not shown). This all shows that Nup145p-C, Nup120p, and Nup85p-C, but not Nup84p and Seh1p are essential for assembly of the Nup84p complex.

Since Seh1p interacts directly with Nup85p (see above; Siniossoglou et al., 1996), we wanted to analyze which part of Nup85p is responsible for this interaction. Therefore, Nup85p truncation constructs lacking either the NH_2-terminal (Nup85pΔN) or COOH-terminal domain (Nup85pΔC) were made and tagged with ProtA to facilitate biochemical purification. To test their functionality, both truncated proteins were transformed into a *nup85::HIS3* deletion mutant lacking the entire *NUP85* ORF. The Nup85pΔN mutant grows well at 30°C, but is thermosensitive at 37°C. In contrast, the Nup85pΔC strain grows extremely slowly at 30°C, and cannot grow above 32°C (Fig. 4 a). Western blot analysis of extracts derived from the strains expressing the Nup85p truncation mutants showed that the two proteins are expressed at similar levels at the restrictive temperature (data not shown). Affinity-purification of ProtA-Nup85ΔNp revealed that all components of the Nup84p complex except Seh1p copurified (Fig. 4 b, Coomassie and Western blot). Conversely, affinity-purified ProtA-Nup85pΔC contained Seh1p, although in reduced amounts, and completely lacked the other four members of the complex (Fig. 4 b). Shorter NH_2-terminal fragments of Nup85p could not be stably expressed in yeast, therefore it was not possible to define the minimal Seh1p-binding sequence within Nup85p. When the distribution of the GFP-Nup49p NPC reporter was analyzed in these mutants, NPC clustering was seen in both Nup85pΔC and Nup85pΔN strains, although clustering was less striking in the case of Nup85pΔN (Fig. 4 c). Furthermore, nuclear mRNA export is severely impaired at the restrictive temperature in both mutants (Fig. 4 d).

These data show that Nup85p contains two distinct domains, a COOH-terminal part, which is required for bind-

Table II. Nup84p Complex Assembly in Nucleoporin Mutants

Strain background	Nup84p-ProtA associated proteins	Seh1p-ProtA associated proteins
nup84::HIS3	Nup85p, Nup120p, Nup145Cp, Seh1p, Sec13p	Nup85p, Nup120p, Nup145Cp, Sec13p
nup120::HIS3	–	Nup85p
nup145ΔC	ND	Nup85p
seh1::HIS3	Nup85p, Nup120p, Nup145Cp, Sec13p	Nup84p, Nup85p, Nup120p, Nup145Cp, Sec13p
sec13-34	ND	Nup84p, Nup85p, Nup120p, Nup145Cp

Assembly of the Nup84p complex in nucleoporin mutants. Nup84p-ProtA or Seh1p-ProtA were affinity-purified from *nup84::HIS3*, *nup120::HIS3*, *seh1::HIS3*, *nup145ΔC*, and *sec13-34* strains. The components, which copurified, are listed in the table. ND, not determined.

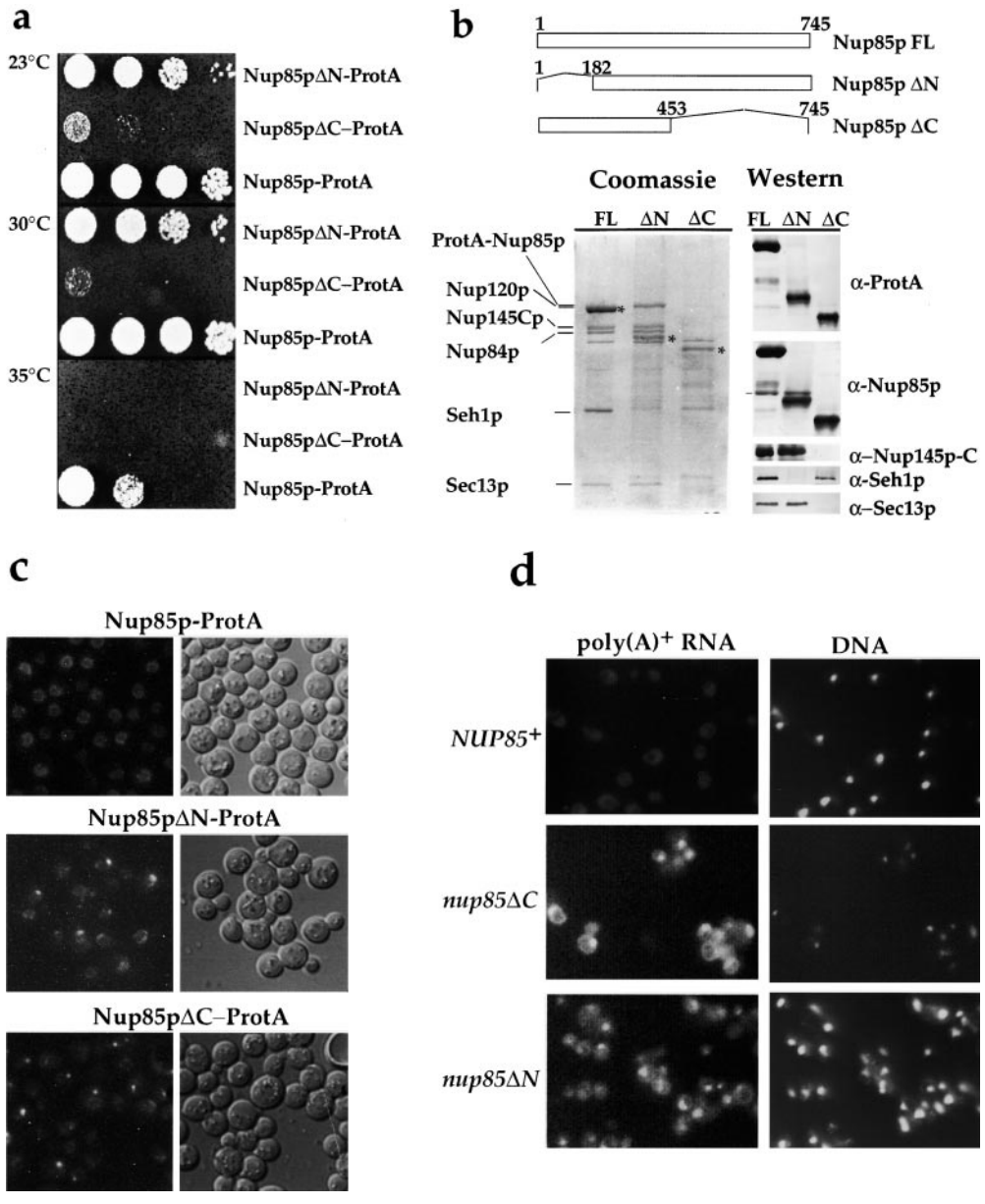

Figure 4. Distinct domains within Nup85p are required for interaction with the various members of the Nup84p complex. (a) Growth of *nup85ΔC* and *nup85ΔN* strains at 23, 30, and 35°C. A *nup85::HIS3* null deletion mutant was transformed with the two *nup85* truncation constructs and the corresponding strains were spotted onto yeast extract–peptone–d-glucose plates at the indicated temperatures. (b) Affinity-purification ProtA–tagged Nup85p full-length (FL) and of the Nup85pΔN (Δ1–182) and Nup85pΔC (Δ453–745) constructs. Shown is a Coomassie-stained gel of the purified complexes (the fusion proteins are indicated by asterisks, and the components of the Nup84p complex by lines), and a Western blot (right panel, only the relevant area from each blot is shown) using anti–ProtA, anti-Nup84p, anti-Nup145Cp, anti-Seh1p, and anti-Sec13p antibodies. (c) Deletion of the Nup85p COOH-terminal domain causes NPC clustering. The corresponding strains were transformed with a plasmid expressing GFP-Nup49p, shifted for 3 h to 37°C and the distribution of this NPC reporter was analyzed in the fluorescence microscope. (d) Both the COOH and NH_2 domains of Nup85p are required for efficient nuclear mRNA export. The *nup85ΔC* and *nup85ΔN* mutants as well as a wild-type control (*NUP85*$^+$) were grown for 3 h at 37°C, fixed, and hybridized with a oligo(dT)-FITC probe to reveal poly(A)$^+$ RNA distribution. Cells were also stained with Hoechst 33258 (DNA).

ing to Nup120p, Nup145p-C, Nup84p, and Sec13p, and an NH_2-terminal part, which binds to Seh1p. Both domains of Nup85p are required for nuclear mRNA export.

The Highly Purified Nup84p Complex Elutes as a Large Assembly during Gel Filtration

In the past and as described above, the affinity-purified Nup84p complex was eluted from the IgG-Sepharose beads through a denaturing low pH treatment (Siniossoglou et al., 1996). To release the purified Nup84p complex from the IgG beads under nondenaturing conditions, the TEV proteolytic cleavage site (a seven amino acid long cleavage site specific for the tobacco etch virus protease) was engineered between the ProtA tag and Nup85p (Fig. 5 a, left panel). This ProtA-TEV-Nup85p fusion construct was functional, since it can complement the *nup85::HIS3* null mutant (data not shown). When ProtA-TEV-Nup85p was affinity-purified as described previously, and the IgG-Sepharose beads were incubated with recombinant TEV protease, cleaved Nup85p was released from the column together with the other members of the complex (Fig. 5, a and b, E1 and E2). However, the cleaved off ProtA moiety remained on the IgG-Sepharose beads. A smaller amount of ProtA-Nup85p that was not cleaved by the protease was eluted from the beads by a final pH 3.5 treatment (Fig. 5 a, HAc).

To further purify the released Nup84p complex, which still contained contaminants such as heat shock proteins, IgGs, and TEV protease (see Fig. 5 b, E1 and E2), and to

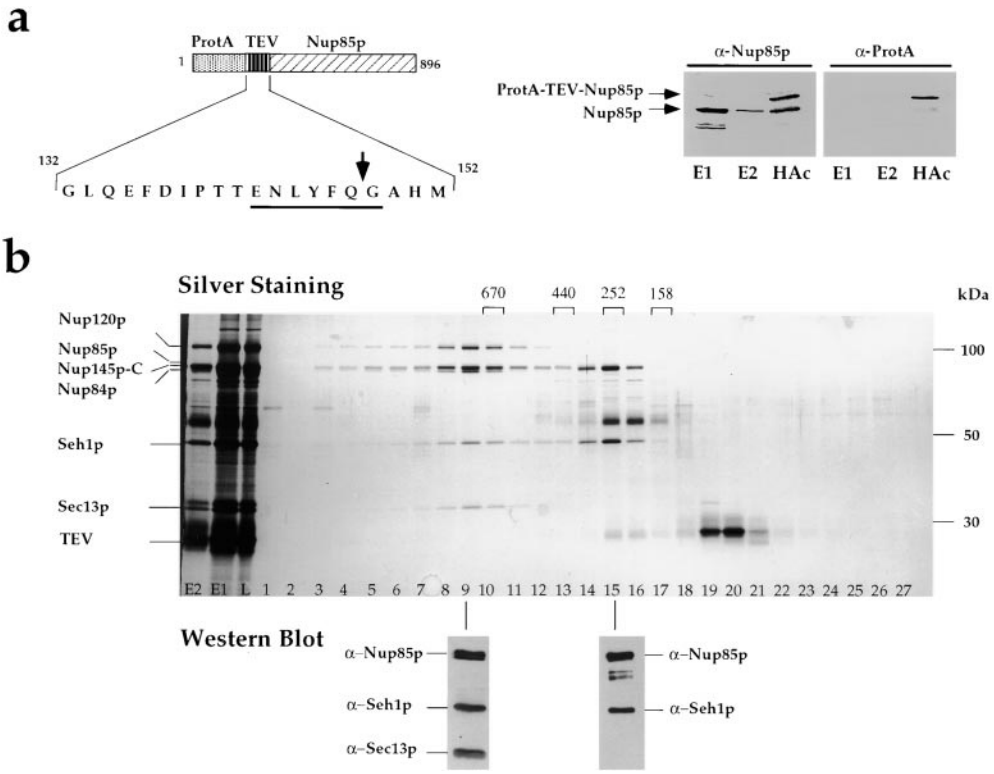

Figure 5. Purification of a native Nup84p complex. (a) TEV protease induced release of affinity-purified ProtA-TEV-Nup85p from IgG-Sepharose beads. Schematic representation of the ProtA-TEV-Nup85p fusion protein consisting of two IgG binding domains (ProtA), a 10 residue long spacer sequence, the 7 residue long TEV cleavage sequence (underlined) with the cleavage site (indicated by an arrow), followed by the Nup85p sequence. After TEV elution from the beads, a first and second eluate (E1 and E2) were obtained. Finally, a low pH eluate (HAc) was collected. All eluates were analyzed by SDS-PAGE and Western blotting using anti-Nup85p and anti-ProtA antibodies. The positions of the ProtA-TEV-Nup85p and the cleaved Nup85p, lacking the ProtA tag are indicated. (b) Gel filtration chromatography of the affinity-purified and TEV-released Nup84p complex. The eluates E1 and E2, which were combined and concentrated to yield the load fraction (L) were analyzed by FPLC Superose 6 column chromatography. 0.6-ml fractions were collected and 25 μl of fractions 1–27, E1 and E2, and the load (L, 5% of the injected material) were analyzed by SDS-PAGE and silverstaining. The six subunits containing Nup84p complex peak in fraction 9, the Nup85p-Seh1p heterodimer in fraction 15. Fractions 9 and 15 were also analyzed by Western blotting using anti-Nup85p, anti-Nup84p, anti-Seh1p, and anti-Sec13p antibodies, respectively. The positions of the components of the Nup84p complex are indicated. Heavy and light IgG chains are evident in fractions 15 and 16, and the TEV protease in fractions 19 and 20. The Superose 6 column was calibrated with several molecular weight marker proteins of 670, 440, 252, and 158 kD (Bio-Rad).

determine its size and structure, the TEV eluate was concentrated by ultrafiltration and applied to an FPLC Superose 6 gel filtration column (see Materials and Methods). SDS-PAGE of the collected fractions revealed that all six components of the Nup84p complex, including Sec13p, exactly cofractionate in only a few fractions, yielding an essentially pure Nup84p complex (Fig. 5 b, fractions 8–10). The column was calibrated with a protein standard of known molecular weight. Accordingly, the Nup84p complex elutes in a peak corresponding to ~700 kD (Fig. 5 b; see below also).

Interestingly, Nup85p and Seh1p form a second peak (Fig. 5 b, fraction 15) that does not contain the other members of the complex (Fig. 5 b; note that these fractions contain IgG heavy and light chains). Accordingly, besides being organized in a large complex, Nup85p and Seh1p can form a heterodimeric complex, which is in agreement with our data described above. Thus, affinity-purification of the Nup84p complex (via tagged Nup85p), its elution from the affinity matrix by TEV cleavage, and final gel filtration chromatography yielded a highly pure preparation of the Nup84p complex.

The Highly Purified Nup84p Complex Exhibits a Y-Shaped Structure and a Molecular Mass of 375 kD

The purified Nup84p complex, which elutes as a large complex as determined by gel filtration chromatography (see also Fig. 5 b), may exhibit a distinct structure that could correspond to one of the above mentioned structural modules of the NPC. To analyze the structure of purified Nup84p complex by EM, both negative staining and glycerol spraying/low-angle rotary metal shadowing were performed. As a sample we used the Nup84p complex preparation derived from the gel filtration column (corresponding to Fig. 5 b, fractions 8–10), which is essentially pure as judged from the silverstained SDS-polyacrylamide gel (Fig. 5 b). This sample of the Nup84p complex yielded a prevalent morphology in the electron microscope. Independent of the applied specimen preparation procedure (i.e., negative staining or low-angle rotary metal shadowing), the Nup84p complex exhibits a predominantly Y-shaped, triskelion-like structure with an overall diameter of ~25 nm (Fig. 6, a and b). In these projections, the Nup84p complex exhibits an approximate mirror symmetry, suggesting that the complex harbors a corresponding twofold axis of symmetry. Although the complexes appear to adsorb with a preferred orientation on the grid, there is a variation in molecular morphology, which indicates a degree of flexibility in the links between the arms and the stalk. Thus, the Nup84p complex may be a rather flexible structure. However, since the preparation is to a certain extent heterogenous in the electron microscope (only ~60% of the negatively stained structures >10–15 nm

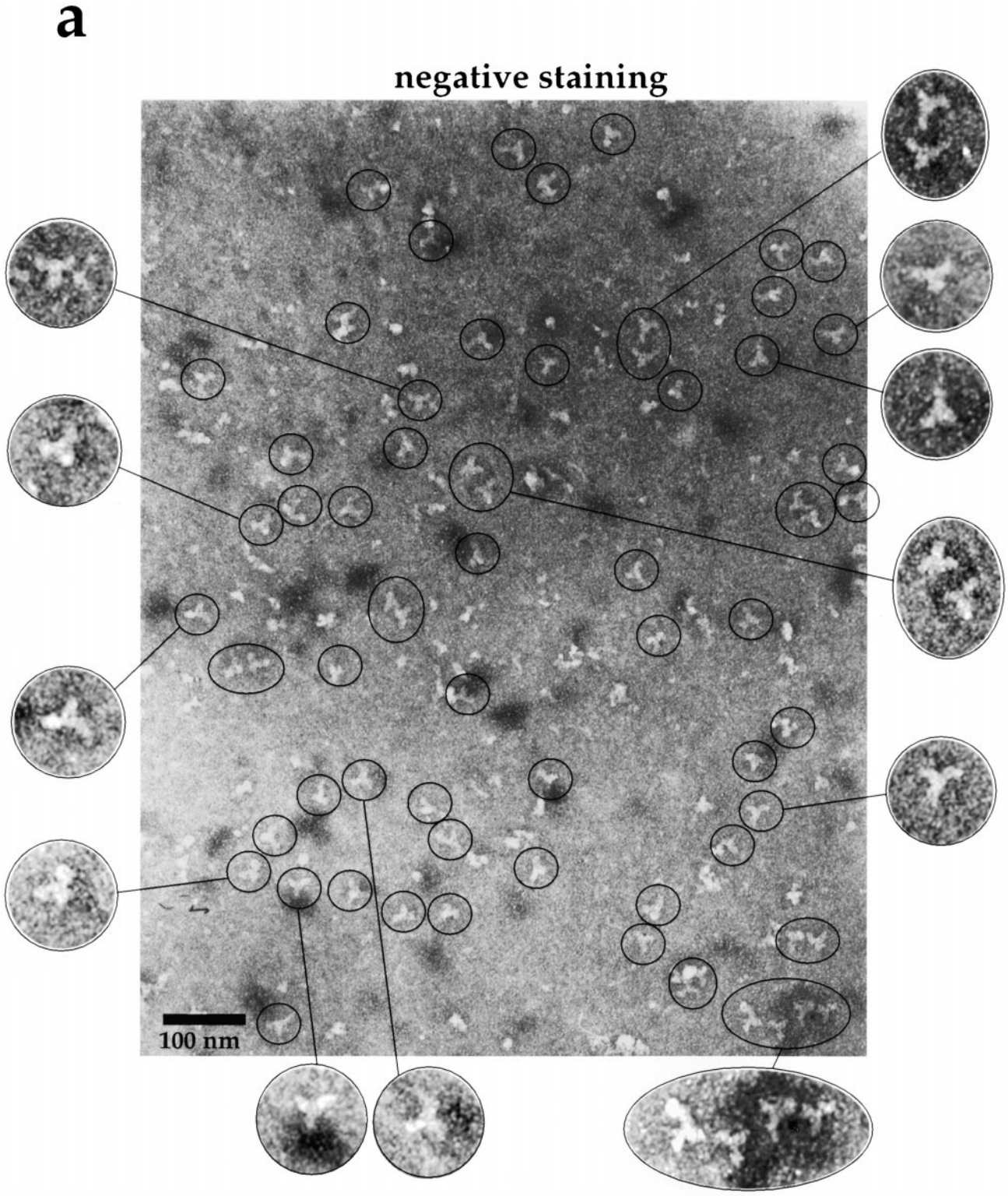

Figure 6 (continues on facing page).

show a Y-shaped form; see Fig. 6 a), it is possible that this is due to partial subunit disassembly during preparation.

According to the gel filtration data, the molecular mass of the Nup84p complex was estimated to be ~700 kD (see Fig. 5 b). This value is almost twice that of the calculated molecular mass of 442 kD, assuming that all six subunits are present in one copy per complex. However, due to its nonglobular Y-shaped structure, the complex may exhibit an abnormal gel filtration behavior. Therefore, we determined the molecular mass of the purified Nup84p complex

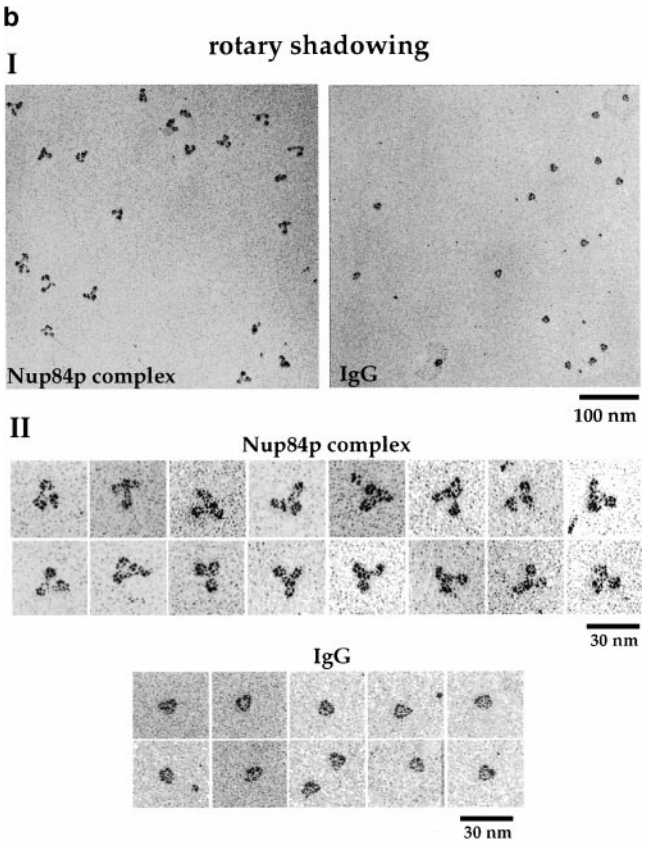

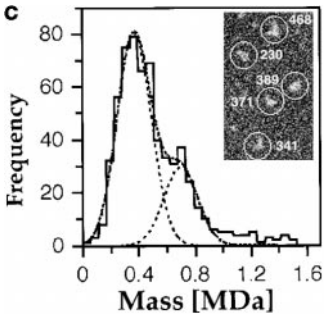

Figure 6. The highly purified Nup84p complex displays a Y-shaped, triskelion-like structure with a molecular mass of ~375 kD. Electron microscopic appearance of the highly purified Nup84p complex after negative staining (a) and glycerol/rotary metal shadowing (b). In a, a large overview picture is shown, on which Y-shaped structures are highlighted by circles. Selected Y-shaped molecules from this picture were further processed by cut and paste and magnification using Adobe Photoshop, and are shown at the edge of the overview picture. In b, overview pictures (I) and a gallery of selected Nup84p particles (II) are shown. For comparison, shadowed IgG particles are also depicted in b. (c) Mass determination of the highly purified Nup84p complex by STEM. Histogram displaying the mass data determined for 619 particles. Correction has been made for beam-induced mass loss. The two Gaussian curves fall at 368 ± 122 kD (n = 438) and 698 ± 123 kD (n = 158), respectively. The number of particles giving rise to the peaks (n) was estimated by measuring up to and away from the point of peak overlap. The inset reveals a field from an annular dark-field image recorded of an unstained freeze-dried Nup84p sample.

by quantitative STEM and analytical ultracentrifugation. Whereas for STEM predominantly particles with a similar average diameter (i.e., 25 nm) as in negative stain were depicted, in unstained freeze-dried samples, the typical Y-shaped, triskelion-like morphology readily observed with negatively stained Nup84 complex was more difficult to delineate in the STEM (Fig. 6 c, inset). Nevertheless, all except the very smallest particles were selected for measurement, and their absolute mass values were calculated, pooled, and displayed in a histogram (Fig. 6 c). This histogram was fitted by two Gauss curves peaking at 368 ± 122 kD (n = 438 particles) and 698 ± 123 kD (n = 158 particles), respectively (i.e., after correction to zero mass loss). To a first approximation, these two peak values indicate the sample to consist of a mixture of a monomeric (~75%) and a dimeric (~20%) Nup84p complex, with a small amount (~5%) of larger (>1 MD) aggregates. However, the standard deviations are too large to simply stem from fluctuations in the background scattering, thus indicating some heterogeneity of the two Nup84p populations. It is conceivable that the bona fide Nup84p complex exhibits a rather limited stability with its more peripheral subunits, having a tendency to dissociate, so that each of the two Gauss curves represents several distinct Nup84p particles, i.e., containing different numbers of subunits.

The highly purified Nup84p complex was also subjected to analytical ultracentrifugation. By sedimentation equilibrium analysis, a predominant species with an average mass of 375 ± 13 kD was depicted at speeds ranging between 6,400 and 8,000 rpm and protein concentrations adjusted to OD_{280} of 1.0, 0.2, and 0.15. The corresponding major $S_{20,w}$ value was 5.6 by sedimentation velocity at 52,000 rpm, an S value being consistent with a flat Y-shaped 375 kD particle as deduced from EM of negatively stained samples (Fig. 6, a and b), mass determination by STEM (Fig. 6 c), and sedimentation equilibrium centrifugation analysis. According to these mass determination data, the Nup84p complex exists predominantly in a monomeric form when isolated from yeast.

Discussion

Now that most of the yeast nucleoporins have been cloned and characterized, the next goal is to put them into a higher order biochemical and structural context. Here, we report on the molecular and structural characterization of the yeast Nup84p complex. This NPC subassembly consists of six subunits, five of which are bona fide nucleoporins (Siniossoglou et al., 1996). When the essential nucleoporins of this complex are mutated, inhibition of nuclear mRNA export and defects in the distribution of NPCs and in the organization of the nuclear membrane occur. In the case of Nup85p, a physical and genetic link to the mRNA export machinery could be shown (Segref et al., 1997; Santos-Rosa et al., 1998), whereas Nup84p genetically interacts with two novel nuclear/ER membrane proteins, Spo7p and Nem1p, required for formation of a spherical nucleus (Siniossoglou et al., 1998). However, the role of the sixth member of the Nup84p complex, Sec13p, a bona fide subunit of the COPII coat complex, remained unclear. We now demonstrate that a pool of Sec13p functions as a nucleoporin.

Several lines of evidence support a role for Sec13p at the nuclear pore. First, we found that a pool of Sec13p-GFP colocalizes with NPCs in a clustering nucleoporin mutant. Apparently, this reflects the same pool of Sec13p, which physically interacts with the Nup84p complex. Second, the distribution of the GFP-Nup49p, which serves as a nucleoporin reporter, is altered in several of the newly isolated ts *sec13* mutants. Strikingly, thin sectioning EM of the *sec13-3*, *sec13-14*, and *sec13-34* cells shifted to the restrictive temperature reveals abnormalities within the nuclear membrane and an accumulation of intracellular membranes, which could be nuclear envelope–attached ER. In addition, NPC herniations arise within the nuclear envelope of *sec13* ts mutants, typically found in other nucleoporin mutants such as *nup116Δ* and *gle2/nup40Δ*. This all shows that Sec13p is required for normal nuclear envelope and NPC biogenesis. Interestingly, another COPII mutant, *sec23-1*, also exhibits defects in the distribution of the GFP-Nup49p nucleoporin reporter. Mutants blocking COPII function accumulate ER membranes at the nonpermissive temperature. Thus, it is possible that the abnormal NPC distribution in the *sec23* and/or *sec13* mutant is due to the accumulation of nuclear pores into these ER membranes, before their incorporation into the nuclear membrane. Alternatively, there might be a more direct link between COPII vesicle budding from the ER and the biogenesis of nuclear pores. Third, two ts alleles, *sec13-14* and *sec13-34*, are synthetically lethal with the *nup85Δ* mutant at 32°C, showing that Nup85p and Sec13p perform overlapping or redundant functions at the NPC. Surprisingly, combined *seh1* and *sec13* mutant alleles do not exhibit such a genetic interaction.

Our biochemical analysis revealed that Nup120p, Nup145p-C, and the COOH-terminal domain of Nup85p are essential for the assembly of a core complex in vivo and thereby may serve as an assembly core or structural scaffold of the complex. Evidently, Nup84p, Seh1p, and Sec13p reside more peripherally within the Nup84p complex. Strikingly, the three members of the core complex exhibit a strong link to the mRNA export machinery (Fabre et al., 1994; Aitchison et al., 1995; Goldstein et al., 1996; Siniossoglou et al., 1996; Teixeira et al., 1997). Hence, it is conceivable that the Nup84p complex consists of a structural scaffold, which at the same time is involved in nuclear mRNA export (e.g., by interacting with mRNA export factors such as Mex67p and Mtr2p; see also Santos-Rosa et al., 1998). In contrast, the more peripheral, dispensable members of the complex (Nup84p, Seh1p, Sec13p) control the distribution of NPCs within the nuclear membrane as well as nuclear envelope organization. In the case of the nonessential Seh1p, we could show that it directly binds to the NH_2-terminal domain of Nup85p as one subunit of the core complex; this interaction is stable up to high salt concentrations (Siniossoglou et al., 1996), and a separate Nup85p–Seh1p heterodimeric complex is even detected in vivo (this study). The role of this heterodimeric Nup85p–Seh1p complex is presently unknown, but it could play a direct role in nucleocytoplasmic transport or represent a stable intermediate during NPC assembly.

The highly purified Nup84p complex exhibits a defined structure as revealed by EM of negatively stained as well as glycerol-sprayed/low-angle rotary metal-shadowed specimens. Although not appearing 100% homogeneous in the EM, >50% of the highly purified Nup84p complex exhibits a distinct Y-shaped or triskelion-like morphology with an overall particle diameter of ~25 nm. We have estimated that there are between 8 and 16 copies of the Nup84p complex per NPC (Lutzman, M., and E. Hurt, unpublished data). Hence, the Nup84p complex makes a significant contribution to the overall mass of the NPC. Because of its apparent twofold symmetry, one possibility is that in situ, the Nup84p complex may assemble into an octagonal ring-like array, for instance, via interaction of the Y-shaped arms of adjacent complexes. In such a model, the third arm of each Nup84p complex unit remains free, and thus could interact with other components of the NPC, for example with a cytoplasmic fibril, and/or with transport factors. Alternatively, the Nup84p complex may oligomerize so that all three arms of a Y-shaped molecule are engaged in binding to other Y-shaped Nup84p complex molecules, thereby forming a coat- or cage-like structure. Finally, we cannot exclude that individual Y-shaped Nup84p particles exist within the structural framework of the NPC. Further structural and biochemical analysis of the Nup84p complex and its organization into higher-order complexes, including identification of its interacting components at the NPC, should help to answer these open questions.

Given the finding that the central NPC framework is conserved from yeast to vertebrates (Yang et al., 1998), it would be predicted that a homologue to the Nup84p complex might also exist in higher eukaryotes. Indeed, a recent study reported the identification of a mammalian NPC subcomplex containing the homologues of cleaved yeast Nup145p-C and Nup84p. Intriguingly, this complex also contains mammalian Sec13p and a Sec13p-related protein showing that the function of Sec13p at the nuclear pore has been evolutionarily conserved (Fontoura et al., 1999). It is therefore conceivable that the overall structure of the NPC is built from distinct subcomplexes or structural modules, which have been conserved during eukaryotic evolution.

In summary, the Nup84p complex appears to be a paradigm for the structural and functional analysis of an NPC subcomplex or a structural module. Amenable to yeast genetics and cell biological methods in vivo, as well as to biochemical purification and EM in vitro, it may be possible to reconstruct its 3-D structure, and to fit, i.e., to position and orient it into a 3-D mass density map of the entire NPC. Last but not least, it may be possible to use the purified Nup84p complex as a seed to reconstitute step-by-step an NPC in vitro from its purified nucleoporins and/or distinct subcomplexes.

We thank Dr. R. Schekman for sending us the *sec23-1* mutant; Sabine Wirz for having recorded the STEM images of unstained/freeze-dried Nup84p complexes used for mass determination; and Ariel Lustig for having performed the analytical ultracentrifugation runs of highly purified Nup84p complexes. The critical proofreading of Katja Sträßer and Olivier Gadal is also acknowledged.

This work was supported by grants from the Deutsche Forschungsgemeinschaft (SFB352 to E. Hurt), the Human Frontiers Science Program (to E. Hurt and U. Aebi), the Swiss National Science Foundation (3100-053034 to U. Aebi), and by the Kanton Basel-Stadt and the M.E. Müller Foundation of Switzerland.

Submitted: 13 October 1999
Revised: 22 February 2000
Accepted: 28 February 2000

References

Aitchison, J.D., G. Blobel, and M.P. Rout. 1995. Nup120p: a yeast nucleoporin required for NPC distribution and mRNA transport. *J. Cell Biol.* 131:1659–1675.

Bailer, S.M., S. Siniossoglou, A.V. Podtelejnikov, A. Hellwig, M. Mann, and E.C. Hurt. 1998. Nup116p and Nup100p are interchangeable through a conserved motif which constitutes a docking site for the mRNA transport factor Gle2p. *EMBO (Eur. Mol. Biol. Organ.) J.* 17:1107–1119.

Barlowe, C., L. Orci, T. Yeung, M. Hosobuchi, S. Hamamoto, N.R. Salama, M.F. Rexach, M. Ravazzola, M. Amherdt, and R. Schekman. 1994. COPII: a membrane coat formed by Sec proteins that drive vesicle budding from the endoplasmic reticulum. *Cell.* 77:895–907.

Belgareh, N., and V. Doye. 1997. Dynamics of nuclear pore distribution in nucleoporin mutant yeast cells. *J. Cell Biol.* 136:747–759.

Bucci, M., and S.R. Wente. 1998. A novel fluorescence-based genetic strategy identifies mutants of *Saccharomyces cerevisiae* defective for nuclear pore complex assembly. *Mol. Biol. Cell.* 9:2439–2461.

Doye, V., and E.C. Hurt. 1997. From nucleoporins to nuclear pore complexes. *Curr. Opin. Cell Biol.* 9:401–411.

Eason, R. 1986. Analytical ultracentrifugation. *In* Centrifugation, A Practical Approach. 2nd ed. D. Rickwood, editor. IRL Press, Washington, DC. 251–286.

Engel, A. 1978. Molecular weight determination by scanning transmission electron microscopy. *Ultramicroscopy.* 3:273–281.

Engel, A., and R. Reichelt. 1988. Processing of quantitative scanning transmission electron micrographs. *Scanning Microsc. Suppl.* 2:285–293.

Fabre, E., and E. Hurt. 1997. Yeast genetics to dissect the nuclear pore complex and nucleocytoplasmic trafficking. *Annu. Rev. Genet.* 31:277–313.

Fabre, E., W.C. Boelens, C. Wimmer, I.W. Mattaj, and E.C. Hurt. 1994. Nup145p is required for nuclear export of mRNA and binds homopolymeric RNA in vitro via a novel conserved motif. *Cell.* 78:275–289.

Fahrenkrog, B., E.C. Hurt, U. Aebi, and N. Panté. 1998. Molecular architecture of the yeast nuclear pore complex: localization of Nsp1p subcomplexes. *J. Cell Biol.* 143:577–588.

Fontoura, B.M.A., G. Blobel, and M.J. Matunis. 1999. A conserved biogenesis pathway for nucleoporins: proteolytic processing of a 186-kilodalton precursor generates Nup98 and the novel nucleoporin, Nup96. *J. Cell Biol.* 144: 1097–1112.

Goldberg, M.W., C. Wiese, T.D. Allen, and K.L. Wilson. 1997. Dimples, pores, star-rings, and thin rings on growing nuclear envelopes: evidence for structural intermediates in nuclear pore complex assembly. *J. Cell Sci.* 110:409–420.

Goldstein, A.L., C.A. Snay, C.V. Heath, and C.N. Cole. 1996. Pleiotropic nuclear defects associated with a conditional allele of the novel nucleoporin Rat9p/Nup85p. *Mol. Biol. Cell.* 7:917–934.

Häner, M., A. Brenner, and U. Aebi. 1997. Glycerol spraying/rotary metal shadowing. *In* Cell Biology: A Laboratory Handbook. J.E. Celis, editor. 2nd ed. Academic Press, San Diego, CA. 292–298.

Kaiser, C., and S. Ferro-Novick. 1998. Transport from the endoplasmic reticulum to the Golgi. *Curr. Opin. Cell Biol.* 10:477–482.

Müller, S.A., K.N. Goldie, R. Bürki, R. Häring, and A. Engel. 1992. Factors influencing the precision of quantitative scanning transmission electron microscopy. *Ultramicroscopy.* 46:317–334.

Murphy, R., J.L. Watkins, and S.R. Wente. 1996. *GLE2*, a *Saccharomyces cerevisiae* homologue of the *Schizosaccharomyces pombe* export factor *RAE1*, is required for nuclear pore complex structure and function. *Mol. Biol. Cell.* 7:1921–1937.

Ohno, M., M. Fornerod, and I.W. Mattaj. 1998. Nucleocytoplasmic transport: the last 200 nanometers. *Cell.* 92:327–336.

Pryer, N.K., N.R. Salama, R.W. Schekman, and C.A. Kaiser. 1993. Cytosolic Sec13p complex is required for vesicle formation from the endoplasmic reticulum in vitro. *J. Cell Biol.* 120:865–875.

Rout, M.P., and S.R. Wente. 1994. Pore for thought: nuclear pore complex proteins. *TIBS (Trends Biochem. Sci.).* 4:357–363.

Salama, N.R., T. Yeung, and R.W. Schekman. 1993. The Sec13p complex and reconstitution of vesicle budding from the ER with purified cytosolic proteins. *EMBO (Eur. Mol. Biol. Organ.) J.* 12:4073–4082.

Santos-Rosa, H., H. Moreno, G. Simos, A. Segref, B. Fahrenkrog, N. Panté, and E. Hurt. 1998. Nuclear mRNA export requires complex formation between Mex67p and Mtr2p at the nuclear pores. *Mol. Cell. Biol.* 18:6826–6838.

Segref, A., K. Sharma, V. Doye, A. Hellwig, J. Huber, R. Lührmann, and E.C. Hurt. 1997. Mex67p which is an essential factor for nuclear mRNA export binds to both Poly(A)$^+$ RNA and nuclear pores. *EMBO (Eur. Mol. Biol. Organ.) J.* 16:3256–3271.

Shah, S., S. Tugendreich, and D. Forbes. 1998. Major binding sites for the nuclear import receptor are the internal nucleoporin Nup153 and the adjacent nuclear filament protein Tpr. *J. Cell Biol.* 141:31–49.

Siniossoglou, S., C. Wimmer, M. Rieger, V. Doye, H. Tekotte, C. Weise, S. Emig, A. Segref, and E.C. Hurt. 1996. A novel complex of nucleoporins, which includes Sec13p and a Sec13p homolog, is essential for normal nuclear pores. *Cell.* 84:265–275.

Siniossoglou, S., H. Santos-Rosa, J. Rappsilber, M. Mann, and E. Hurt. 1998. A novel complex of membrane proteins required for formation of a spherical nucleus. *EMBO (Eur. Mol. Biol. Organ.) J.* 17:6449–6464.

Stoffler, D., B. Fahrenkrog, and U. Aebi. 1999. The nuclear pore complex: from molecular architecture to functional dynamics. *Curr. Opin. Cell Biol.* 11: 391–401.

Strambio-de-Castillia, C., G. Blobel, and M.P. Rout. 1999. Proteins connecting the nuclear pore complex with the nuclear interior. *J. Cell Biol.* 144:839–855.

Teixeira, M.T., S. Siniossoglou, S. Podtelejnikov, J.-C. Bénichou, M. Mann, B. Dujon, E. Hurt, and E. Fabre. 1997. Two functionally distincts domains generated by in vivo cleavage of Nup145p: a novel biogenesis pathway for nucleoporins. *EMBO (Eur. Mol. Biol. Organ.) J.* 16:5086–5097.

Terzi, E., G. Hölzemann, and J. Seelig. 1994. Reversible random coil-β-sheet transition of the Alzheimer β-amyloid fragment (25-35). *Biochemistry.* 33: 1345–1350.

Wente, S.R., and G. Blobel. 1993. A temperature-sensitive *NUP116* null mutant forms a nuclear envelope seal over the yeast nuclear pore complex thereby blocking nucleocytoplasmic traffic. *J. Cell Biol.* 123:275–284.

Yang, Q., M.P. Rout, and C.W. Akey. 1998. Three-dimensional architecture of the isolated yeast nuclear pore complex: functional and evolutionary implications. *Mol. Cell.* 1:223–234.